The influence of brace to chord rotational connection stiffness on stability of the truss

Marcin Krajewski[1]

[1] Gdansk University of Technology, Faculty of Civil and Environmental Engineering, Department of Structural Mechanics

Abstract.. The paper is devoted to the numerical analysis of the roof truss subjected to upward wind loading and braced at the tensioned top chord. The linear buckling analysis were performed for the beam and shell model of the structure. As the result the influence of rotational connection stiffness between the brace and the top chord on the truss stability was appointed. The bi-axial strength testing machine was used to conduct the experimental tests of the rotational connection stiffness between selected steel profiles. The results in the form of measured structural displacements and rotations were presented. The static nonlinear analysis results performed for the shell model of the structural connection were compared to the results obtained on the experimental set-up.

Key words: truss, stability, connection, rotational stiffness

1. INTRODUCTION

The flat trusses are often designed as the roof girders in a large span civil engineering buildings. The characteristic feature for that type of structures is high stiffness and load bearing capacity but only in their plane. In the perpendicular direction (out of plane) the braces are designed to ensure the truss stability. There are many types of bracing systems described in literature. The main role of these lateral supports is to restrain the out of plane deformations of the roof structure. The braces are designed (among others) to carry out the horizontal load caused by wind. However, it should be point out that these elements are also subjected to so called imperfection load [1,2]. This horizontal load results from the vertical load subjected to imperfect truss. In this case the load magnitude depends on the distribution of normal forces in the compressed chord [3,4,5] and the imperfection shape of the girder [6].

In many cases in order to simplify the design process the braces are assumed to be rigid. As a consequence the buckling length of the compressed top chord (for the gravity load) or bottom chord (for the wind suction) is assumed as a distance between the lateral supports. The lattice failure (buckling at the bottom chord) caused by the wind was the subject of analysis presented in [7]. The studies on the influence of elastic brace stiffness on truss stability were performed numerically [8,9,10,11] and experimentally [12,13,14]. In these researches the steel structures described by different geometry, cross-section types and boundary conditions were considered. Also the brace translational (out of plane, k) and rotational stiffness (k_{rot}) was taken into account. As one of the results the relation between the external loads and the truss top chord translations (out of plane) and rotations (torsion) was obtained. Moreover, it is

worth noting that the truss capacity was also depended on the initial geometric imperfections [15,16].

Based on the analytical solutions presented in [17] it can be concluded that the properly designed connection between the brace and the top chord significantly affects the structure bearing capacity. In case of wind loading the diagonals are the natural intermediate supports for the compressed bottom chord. These elements can be treated as the elastic foundation for the compressed element. However, in this case the bottom chord buckling length depends not only on the bending stiffness (out of plane) of the diagonals and the torsional stiffness of the tensioned top chord. It also depends on the brace rotational stiffness. The rotational stiffness of the truss side supports results from the bending stiffness of the purlin and the rotational connection stiffness between the purlin and the top chord [17] Eq. (1).

$$\frac{1}{k_{rot}} = \frac{1}{K_{roof}} + \frac{1}{K_{con}} \qquad (1)$$

where: k_{rot} – rotational stiffness of lateral support, K_{roof} – bending stiffness of the brace, K_{con} – rotational connection stiffness between the brace and the truss top chord

Based on the numerical analysis results the rotational brace stiffness affects the imperfection load (horizontal stabilizing forces) mentioned above [6]. The research on the connection stiffness between the steel roof profiles and the trapezoidal sheeting including the design details implementation to the numerical model were presented in [18].

*e-mail: markraje@pg.edu.pl

The present paper is focused on stability studies of the braced truss. The structure presented previously in [17] was taken into consideration. However, the continuous braces along the top chord length (corrugated sheet) was replaced by the lateral point supports located at selected nodes. The truss subjected to upward wind loading was taken into account. The analysis were conducted for the structure without any additional braces located at the compressed bottom chord. The rotational stiffness for the selected connection type (brace to chord) was tested experimentally which is the main part of the presented research. The results obtained on the prototype experimental set up were used to validate the numerical (shell) models of the structural connection. Based on numerical analysis results the influence of brace rotational stiffness on the truss buckling load was presented.

2. DESCRIPTION OF THE TESTED STRUCTURES

2.1. Numerical model of the truss

The model of steel flat truss loaded at braced top chord joints was taken into consideration (Fig.1). The analysis of the similar structure were presented previously in [17], however in the current parametrical studies the braces in the form of elastic point supports (purlins) were taken into account instead of bracing system in the form of trapezoidal sheet. The truss length was $L=15.0$ m and the depth $h=0.7$ m. The separate members of the structure were made of rectangular bars: top chord - RHS 120x100x4, bottom chord RHS 100x100x4, diagonals RHS 50x50x3. The truss was made of steel S355. Based on the standard requirements [1] the following material parameters were assumed: Young's modulus $E=210$ GPa, Poisson's ratio $v=0.3$ and the yield strength of the steel $f_y=355$ MPa.

The finite element method was used to perform the stability analysis for the spatial (beam and shell) models of the structure defined in *Femap with NX Nastran* software [19] (Fig.2). About 400 beam elements with six degrees of freedom at node were used. The truss elements were connected at joints by means of rigid links. The load (upward wind loading) was applied in the form of concentrated forces located at the top chord braced joints. The braces (purlins) were modeled in the form of side supports (*Dof-spring* elements [19]) characterized by translational (k) and rotational stiffness (k_{rot}).
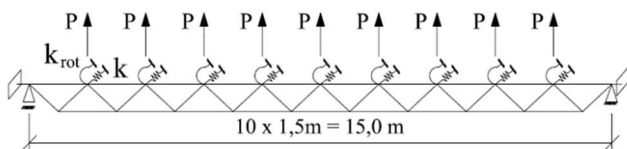

Fig.1. Static schema

The shell model of the structure was created on the basis of the detailed design project. In this case about 34 000 4-node shell elements (*Quad4* [19,20], six degrees of freedom at node, one Gauss point) were used. All eccentric connections between the separated truss members were taken into account. The rigid elements were defined as the replacement for welded connections between diagonals and chords.

The model of the truss was loaded and supported at the selected top chord joints. In this case the intermediate (lateral) and marginal supports and also the concentrated forces were applied to the nodes defined in the center of gravity of the RHS 120x100x4 profile. These reference nodes were rigidly connected with the selected nodes located around the cross section perimeter of the rectangular bar.

It the present research it was assumed that the intermediate supports were rigid by means of out of the truss plane translation ($k=10^6$ kN/m). In the parametric studies the influence of the rotational brace stiffness (k_{rot}) on the truss buckling load was considered. The structure with two different variants of bracing system was taken into account. In the first case each top chord joint was braced (distance between the braces was $L_{br}=1.5$ m). In the second case the distance between the marginal supports and braces and also the distance between the braces was equal to $L_{br}=3.0$ m. The truss was pinned at the marginal supports.

Before the target numerical analysis started (linear buckling analysis, solving the matrix eigenvalue problem) the both described above models of the truss were calibrated by means of mesh density. At the first step each separated member of the structure was divided on two parts (beam model - model A). In the next step 10 finite elements per member were used (Fig.2a, model B). In the last step 100 finite elements were applied (model C). Due to the analysis results the differences in buckling load magnitudes were less than 5% as a comparison between model B and C. On this basis the target analysis were performed for model B of the truss (Fig.2a). The similar research were carried out for the shell model of the structure. In this case at the first step the rectangular profiles were divided on 2 finite elements along cross section height and depth. In the next step (mostly) the dimensions of square elements were about 20 x 20 mm (Fig.2b). The shell model of the truss built of 5.0 x 5.0 mm square elements was also tested. Based on the obtained results the model presented in Fig.2b was chosen to perform the stability analysis for the shell structure.
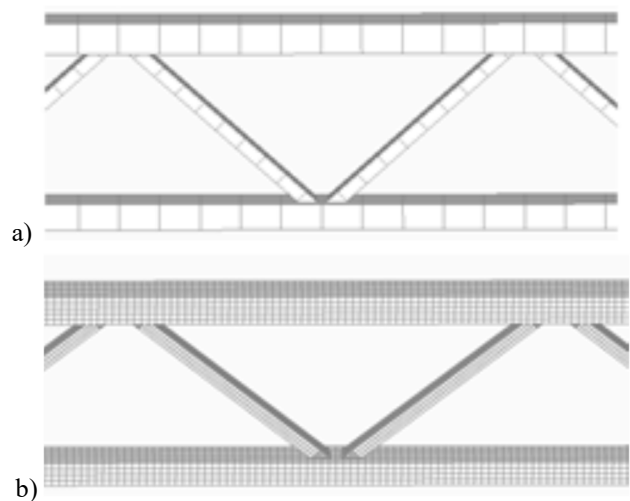

Fig.2. Numerical model details: (a) beam model, (b) shell model

2.2. Details about the tested structural connection

The connection between the truss top chord and the purlin was taken into consideration. In this case the experimental tests and numerical analysis of the connection stiffness between the RHS 120x100x4 profile (part of the truss top chord, S355, length L_{ch}=1.5 m) and IPE100 (part of the purlin, S355, length L_p=0.75m) were performed. The middle of the I-beam was located in the middle of the rectangular bar. The contoured gusset plates (S275, thickness 4.0 mm, located at both sides of the I-beam) and screws (M8, 8.8 class) were used to enable the connection between the main profiles situated one on top of the other (Fig.3, Fig.4).
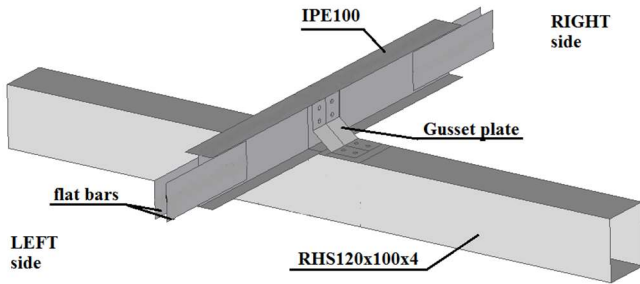

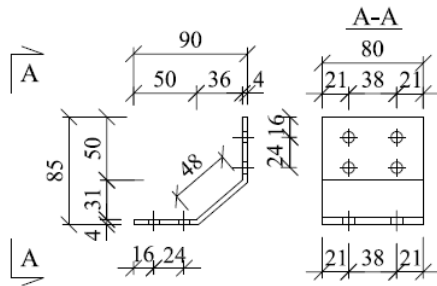**Fig.3.** Structural connection

Fig.4. Gusset plate detail

The bi-axial strength testing machine [21] was used to conduct the experimental tests. In each case the sample was situated on the experimental set-up at the initial angle α=10° (Fig.5). The both ends of the RHS 120x100x4 profile were fixed to the additionally designed steel frames. The loading was applied (at the same time) to the both ends of the I-beam. The steel handles attached to the moving travers (at both opposite sides) were used to combine the tested specimen with the machine (Fig.6). The handles were pinned to the flat bars which were connected with the IPE100 profile. The distance between the hinges was L_b = 0.93 m.
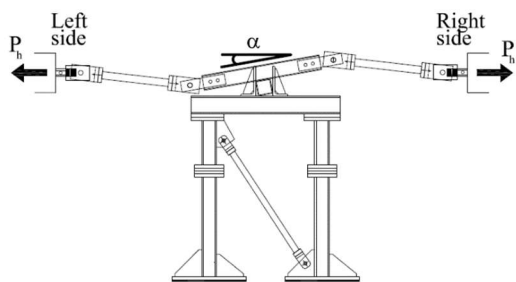

Fig.5. The sample test positioning and load application

Fig.6. Experimental set-up

Based on the loading schema (Fig.7) one can conclude that during the experiment the samples were subjected to tension and bending. It is worth noting that the rotational stiffness of the connection between the rectangular bar and the I-beam was obtained based on the load corresponding to bending. The four samples were tested experimentally. The maximum applied horizontal load (P_H, Fig.5) indicated by the machine force gauges was 18 kN. According to the loading procedure at the first step of the experiment the samples were loaded up to 1.0 kN. In the next step the load decreased to 0.5 kN. In each case this process was needed to avoid the gaps between the set-up components. In the next stage the target measurements started and the test speed was 1.0 kN/min.
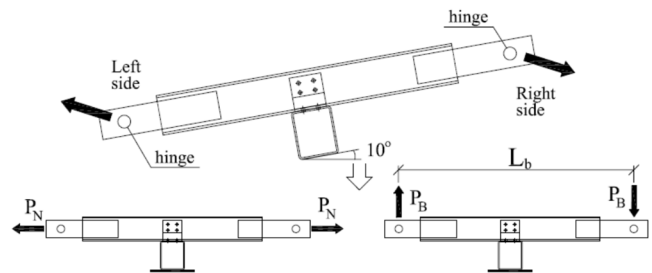

Fig.7. The load application details

During the test the horizontal displacements of the travers (independently at both ends, Fig.5) and the applied load was recorded by the strength testing machine devices [21]. The rotation angle of the sample was also measured by the inclinometers [22] connected to the recording devices [23]. The inclinometers were situated at a distance of 0.15m from the ends of the I-beam (Fig.8). The measurement frequency was 50 Hz and the accuracy was 0.01 degree.

For selected points located on the tested structure the strains were also measured. The strain gauges (Sg1-Sg4) were located in the middle of the I-beam web and also in the middle of the top or bottom shelf of the profile (Fig.9). The sensors were installed at both profile ends (on the left connection side and on the right side). In this case the recording amplifier [24] was used and the measurements frequency was 50 Hz. Due to the results obtained from the sensors the bending load (P_B) and the tensile load (P_N) subjected to the tested sample could be obtained. In this case the calculations were made on the basis of equation (2) and equation (3) for the sensors located on the right side of the connection (ε_1 from Sg1, ε_2 from Sg2). In order to determine the load magnitudes (P_B, P_N) on the left side the strains ε_3, ε_4 (from Sg3 and Sg4 adequately) were taken into account.

3

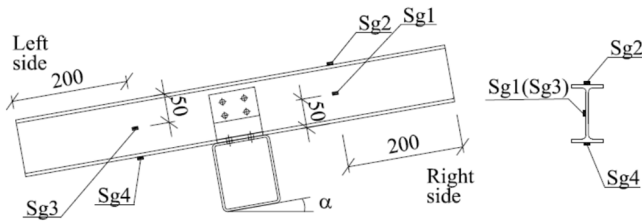**Fig.8.** The inclinometers location on the tested specimen

Fig.9. The location of the strain gauges (Sg1-Sg4) on the purlin

$$P_N = EA\varepsilon_1 \qquad (2)$$

where: P_N – load corresponding to sample tension (on the right side), E- Young's modulus, A- cross section area of the I-beam, ε_1 - strains measured by Sg1 strain gauge

$$P_B = \frac{EW}{L_{Sg}}(\varepsilon_2 - \varepsilon_1) \qquad (3)$$

where: P_B – load corresponding to sample bending (on the right side), W - moment of cross section resistance, L_{Sg} – distance between the hinge and strain gauge Sg1 (0.29 m), ε_2 - strains measured by Sg2 strain gauge

The finite element method was used to perform the static nonlinear analysis [25] for the tested structure. About 11000 shell elements (*Quad* [19,20], three and four nodes elements with six degrees of freedom at node and one Gauss point) were used to define the separate members of the structural connection (Fig.10). In most cases the element side length was up to 0.01m along the walls of the steel profiles and gusset plates. The rigid elements (handles) were implemented to the numerical model as the connection between the tested specimen and the strength testing machine servomotor. The pinned supports with the possibility of sliding (in the horizontal direction) were modeled on one of the ends of the mentioned above rigid elements. On the other side, due to the design project, the connection between the handles and the flat bars (joined with IPE100 profile) was pinned (Fig.5). In the numerical model the load in the form of concentrated forces was introduced. These horizontal forces (with opposite turns) were applied to the supports described

above. The structure was also supported in perpendicular direction. In this case in the first step the rigid links [19] were modeled between the walls of the rectangular bar and the node located at the centre of gravity of the profile (at both profile ends). In the next step the fixed supports were defined in these two reference nodes. It should be also point out that in the numerical analysis the contact surfaces were taken into account. The friction was defined between the bottom shelf of the IPE100 and the top shelf of the RHS120x100x4. Also the connection was defined between the gusset plates and the profiles mentioned above. The assumed kinematic friction coefficient was equal to 0.5. In the numerical model the separate members of the structure were also connected by means of beam elements (circular bar elements, diameter 8 mm, six degrees of freedom at node [19]) located at the holes for bolts. In the analysis the bi-linear elasto-plastic steel model [25] was taken into account (E, f_y due to the standard requirements [1]).
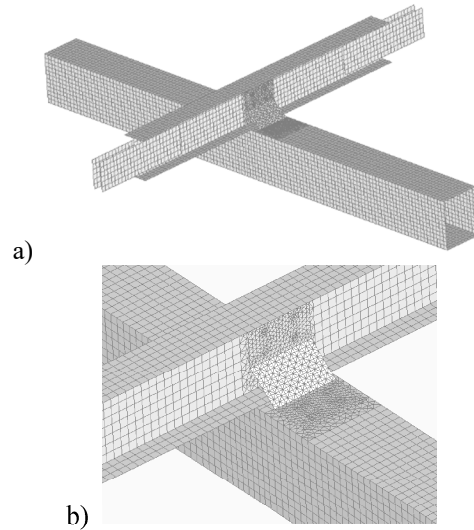

a)

b)

Fig.10. Shell model of the connection: (a) general view, (b) detail of the gusset plate

3. ANALYSIS RESULTS

3.1. Numerical analysis results for the truss

The linear buckling analysis (LBA) were performed for the beam and shell model of the structure. The truss was loaded and braced ($k=10^6$ kN/m and k_{rot}) in every top chord node (variant I, L_{br}=1.5 m) or in every second top chord node (variant II, L_{br}=3.0 m). As the result the buckling load and the corresponded buckling modes were obtained (Fig.11, Fig.12, Fig.13). Based on the results one can conclude that the magnitude of load depended on the rotational stiffness of the lateral supports. In most cases the increase of brace stiffness caused the increase of buckling load. However, there was the threshold brace stiffness above which the load did not raised or the load increase was small (less than 10%). For the tested structure this threshold rotational stiffness of the side supports was equal to 75 kNm/deg (for the beam or shell model).
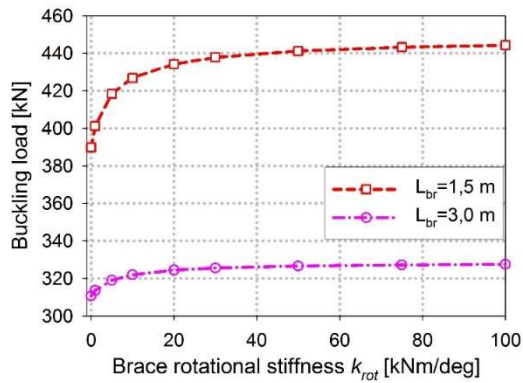
4

Fig.11. The relation between the buckling load and the brace rotational stiffness for the beam model (with respect to distance between the lateral supports, L_{br})
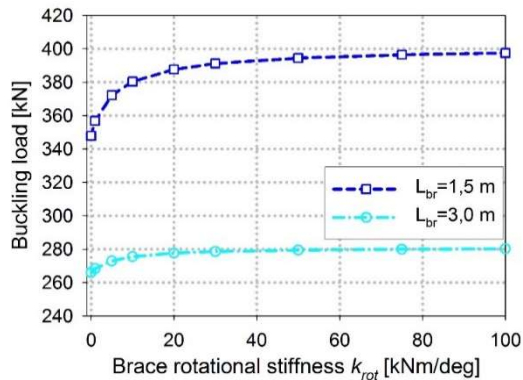

Fig.12. The relation between the buckling load and the brace rotational stiffness for the shell model (with respect to distance between the lateral supports, L_{br})
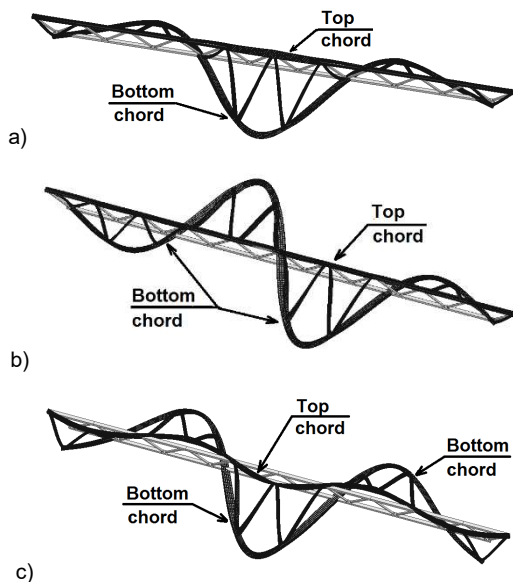

Fig.13. The buckling modes of the truss (shell or beam models) with braces of stiffness ($k=10^6$ kN/m): a) $k_{rot}= 0$ kNm/deg, $L_{st}= 1.5$ m, b) $k_{rot}= 10^6$ kNm/deg, $L_{st}= 1.5$ m, c) $k_{rot}= 0$ kNm/deg or $k_{rot}= 10^6$ kNm/deg, $L_{st}= 3.0$ m

Moreover, it is worth noting that the compressed bottom chord did not buckle in one half-wave (Fig.13) even if the rotational

*e-mail: markraje@pg.edu.pl

brace stiffness was omitted (top chord braces rigid for out of plane translation, $k=10^6$ kN/m and $k_{rot}=0$ kNm/deg). It means that for the tested structure (without any additional supports located at the bottom chord) buckling length of the bottom chord was in each case (beam or shell models) lower than the length between the marginal supports. The buckling mode in the form of one half-wave at the compressed chord appeared only if the brace translational stiffness was $k<100$ kN/m (and $k_{rot}=0$ kNm/deg, $L_{br}=1,5$m). The similar analysis results performed for the steel flat trusses were presented previously in [10,11,14]. The stiffness of the diagonals (out of plane) also affects the buckling length of the bottom chord [17]. These elements supported by the top chord were the elastic foundation for the compressed bottom chord. In this case also the closed cross section shape of the top and bottom chord (torsional stiffness) had the significant influence on the magnitude of buckling load in comparison to the structures made of profiles with built-up or opened cross section [14,15].

In the present research the buckling load raised up to 12% for the shell model or 13% for the beam model due to the increase of the rotational support stiffness. It should be point out that the greatest increase in buckling load occurred for the low magnitudes of the rotational support stiffness. The maximum load magnitude obtained for the shell model of the truss was about 10% lower in comparison to the beam model. In this case the reason for the discrepancies were the differences in structural details modeling (e.g. diagonal to chord connections, boundary conditions) described in the previous section.

3.2. Experimental and numerical analysis results for the tested structural connection

The main purpose for conducting the experimental research was to determine the angle of rotation for the tested I-beam (supported by the rectangular bar) caused by the application of horizontal forces. Based on the obtained results the validation of the numerical shell model was carried out and in the next step the rotational connection stiffness was calculated. In each case the increase of load caused the increase of horizontal displacements of the tested structure (with handles, Fig.14, Fig.15).

The further research result which was observed on the experimental station was the decrease of the initial rotation angle of the sample (10 deg) caused by the load implementation. Before the tests started the values measured by the inclinometers were set to zero and therefore the raise of the rotation angle was recorded during the experiment (Fig.16). As the load increased the I-beam and the handles become straightened to each other. However, based on the presented results, even for the highest load magnitude (18 kN) the I-beam did not reach the horizontal position and the rotation angle was up to 6.0 deg.

During the experiment the stresses obtained on the left and right side of the I-beam (based on strains, Fig.9) raised due to the increase of horizontal load (P_H). These values measured at the maximum load level did not exceed the yield strength of the steel. The load applied perpendicularly to the longitudinal axe of the I-beam (bending load, P_B) and also the tensile load

(parallel to the longitudinal axe of the I-beam, P_N, Fig.7) were calculated on the basis of the measured strains due to the equations (2) and (3). At the same time the rotation of the I-beam was measured. In this case as the result the relation between the bending load or the tensile load (acting on the left or the right side of the specimen) and the rotation of the I-beam was obtained (Fig.17, Fig.18). On this basis the relation between the bending moment ($M=P_BL_b$, averaged bending load on the left and ride side of the connection) and angle of the rotation (ϕ) was determined (Fig.19).
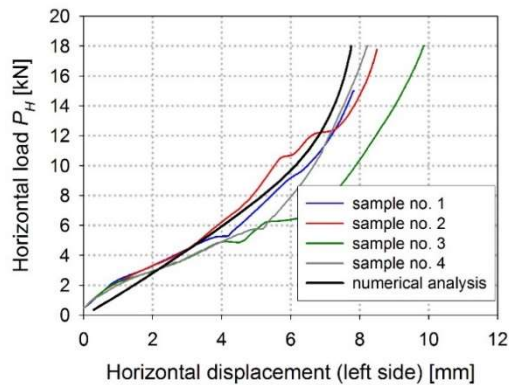

Fig.14. The relation between the horizontal load (P_H) and the horizontal displacements measured on the end of the handle on the left side of the experimental set-up
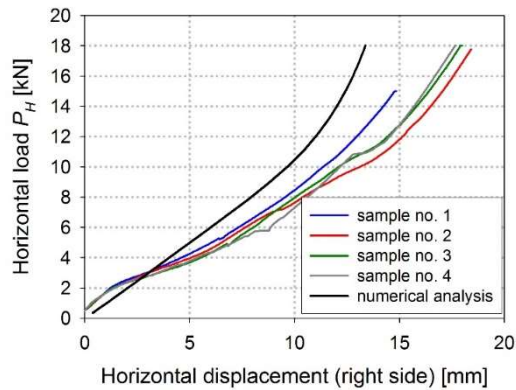

Fig.15. The relation between the horizontal load (P_H) and the horizontal displacements measured on the end of the handle on the right side of the experimental set-up
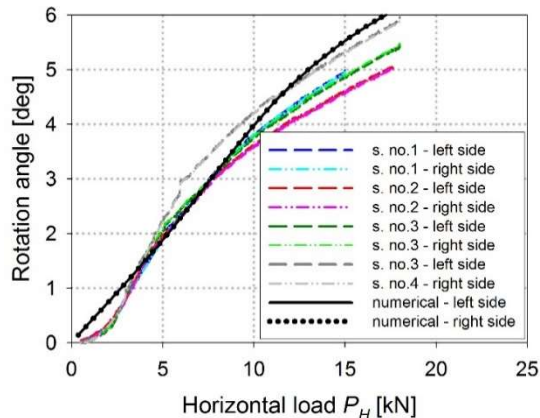

Fig.16. The relation between the angle (ϕ) of the I-beam rotation measured on the left or right side of the profile and the horizontal load (P_H) (experimental and numerical analysis results)
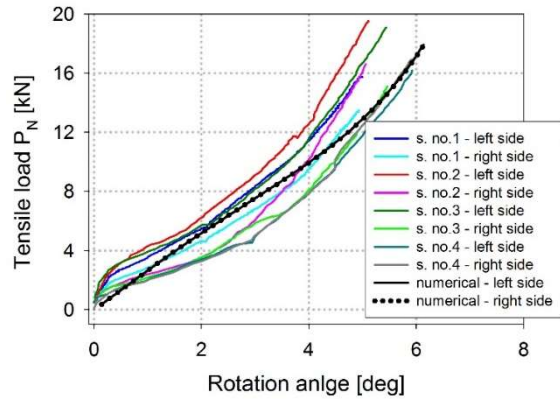

Fig.17. The relation between the tensile load (P_N, measured on the left or right side of the tested sample) *and the angle (ϕ) of the I-beam rotation (experimental and numerical analysis results)*

Fig.18. The relation between the bending load (P_B, measured on the left or right side of the tested sample) *and the angle (ϕ) of the I-beam rotation (experimental and numerical analysis results)*
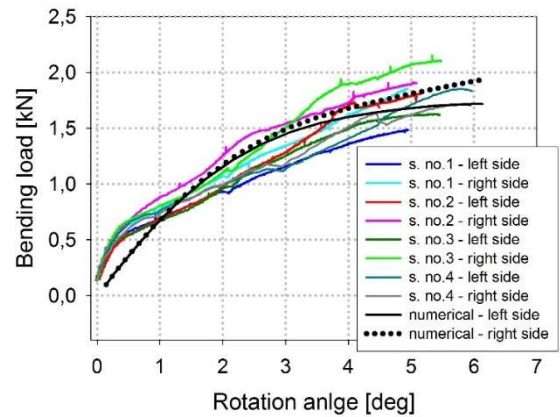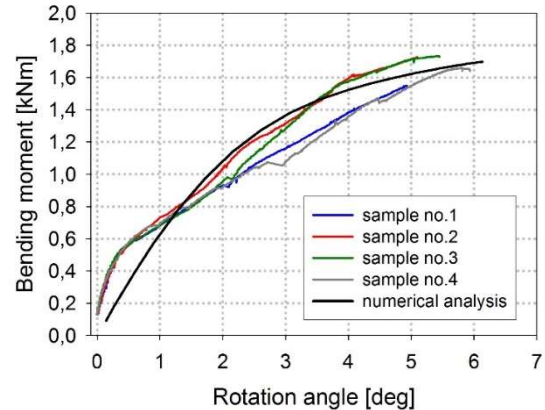

Fig.19. The relation between the bending moment (*M) and the angle (ϕ) of the I-beam rotation (experimental and numerical analysis results, gusset plates thickness 4 mm)*

Due to the method of load transformation from the strength testing machine to the sample the increase of bending load was non-linear. Under the highest horizontal loads (caused by the machine servomotors) the increase in bending load was the lowest which was significantly influenced by the angle of sample rotation (Fig.18).

6

Moreover, it should be point out that at the beginning of the experiment there was the contact surface between the walls of the steel profiles (between the bottom shelf of the I-beam and the top wall of the rectangular bar). However, during the experiment, left side of the I-beam (Fig.5) was lifted relatively to the rectangular bar and the right side was pressed against the bar. It was the reason for the increase of gap between the separated profiles due to the increase of load. On this basis during the tests the bottom shelf of the I-beam was connected only to the edge between two perpendicular walls of the tube (by the right side of the connection). In this case the support line for the IPE100 profile was formulated. On this basis one can conclude that the distance between the support line (mentioned above) and the bending force on the left side of the I-beam was greater in comparison to the corresponding distance on the right side. That is the possible explanation for the slight differences in load components (bending load) on the left and right side of the connection (Fig.18). Moreover, the geometric imperfections (caused by element assembly, not included in the numerical model) might affect the obtained experimental results (Fig.17, Fig.18).

Due to the load application the gusset plates connected with the steel profiles by several bolts (Fig.3, Fig.4) were subjected to tension on the left side of the connection and to compression on the right side. During the tests the shearing of the screws was not noticed in any case. It was observed that the both steel sheets were deformed symmetrically in relation to the I-beam (Fig.20). Due to the limited capabilities of the machine [21] in terms of the maximum load level, the gusset plates used for the experimental tests were made of thin 4 mm sheets. In this case, based on the numerical analysis results the stresses equal to the yield stress of the steel (f_y=275MPa, [1]) appeared on the outer (tensioned) edge of the gusset plates for the horizontal load equal to 4 kN.

According to the results presented in Figure.19 the linear approximation was provided for each of four samples (for the limited load range from 0.6 kNm to 1.6 kNm). Based on these calculations the averaged rotational connection stiffness (constant, $K_{con}=M/\phi$) equal to about 0.3 kNm/deg was obtained. However it should be point out that this stiffness magnitude was found experimentally assuming that both the I-beam and the rectangular bar were flexible. In order to determine the rotational connection stiffness described in equation (1) the further analysis were taken into consideration. In the next step it was assumed that both steel profiles mentioned above were rigid. In this case based on the nonlinear analysis results (GMNA) performed for the validated shell model of the structural connection (gusset plates 4 mm thickness) the rotational stiffness equal to 2 kNm/deg was obtained. However, this stiffness magnitude was calculated for the low range of rotation angle (up to 0.5 deg, Fig.21). For the larger angles the stiffness decreased. Based on the numerical analysis results (Fig.21) the increase of gusset plates thickness did not result in significant changes of the connection stiffness. The average stiffness of the connection was equal to about 1 kNm/deg for the steel sheets of thickness 5 mm (up to the rotation angle equal to 2 deg) and 6 mm (up to the rotation angle equal to 2.5 deg).

In this cases, similarly to the gusset plates tested experimentally, for larger rotation angles the connection stiffness decreased. Based on the numerical analysis results (LBA) the truss buckling load raised up to 3% due to the implementation of the side supports of stiffness equal to krot=1.0 kNm/deg (in comparison to the pinned connection).
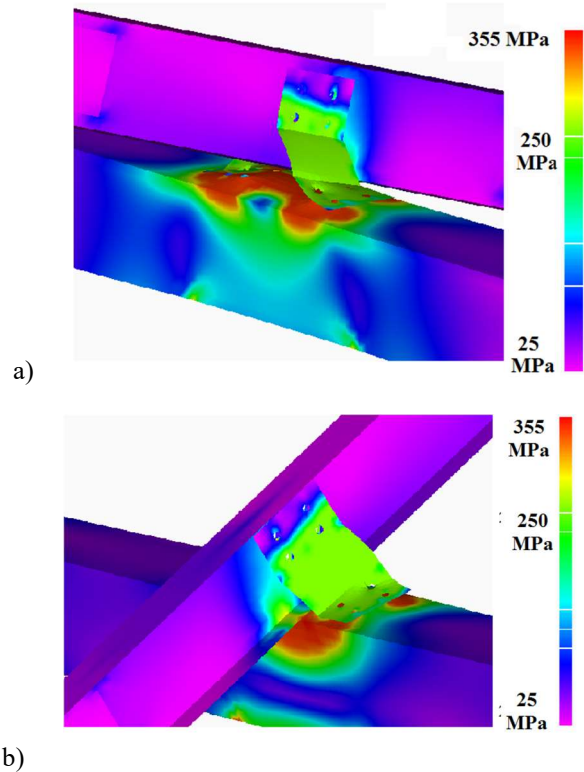

a)

b)

Fig.20. The deformation and the stress state (HMH hypothesis, top surface of the shell model element) at the limit load for the structural connection: a) view form the left side, b) view from the right side
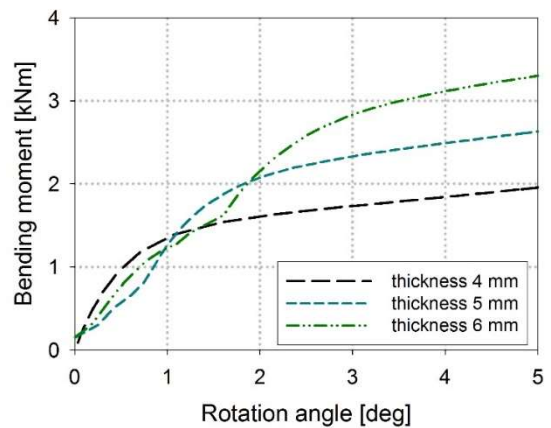

Fig.21. The relation between the bending moment (*M) and the angle (ϕ) of the I-beam rotation relative to the rectangular bar (both rigid profiles) with respect to the thickness of the gusset plates*

4. CONCLUSIONS

In the present research the model of braced roof truss was taken into consideration. On the basis of numerical analysis results (LBA) conducted for the beam and shell model of the structure one can conclude that the buckling load depended on the brace rotational stiffness. In most cases the buckling load raised due

7

to the increase of side support stiffness. However there was the threshold brace stiffness above which the load did not increase or the increase was low (less than 10%). The critical load obtained for the shell model of the truss was about 10% lower in comparison to the beam model (rigid braces). In this case the possible explanation were the differences in modeling of structural details (boundary conditions, connections between separated members). On the basis of buckling modes one can conclude that the buckling length of the compressed bottom chord was in each case lower than the length between the marginal supports. The brace stiffness and the bending and torsional stiffness of the diagonals and top chord (closed cross sections) significantly influenced the magnitude of the truss buckling load.

The experimental tests results and numerical analysis results (shell model, GMNA) obtained for the described structural connection were comparable. The reason for the discrepancies might be the boundary conditions applied to the section of the upper chord in the numerical analysis (fixed supports at both ends of the rectangular bar). Also in the numerical model the initial geometric imperfections of the tested steel profiles including assembly conditions were not taken into account.

Based on the obtained results it can be concluded that the significant deformations occurred on the gusset plates. Due to the increase of load the plasticization range appeared and raised on the surface of these elements. Moreover it should be point out that during the tests not only the I-beam but also the rectangular bar was subjected to displacements and rotations. The length of the tested section of the top chord had the significant impact on the amount of deformation. The validation of the numerical models was performed due to the experimental test results. On this basis the rotational connection stiffness between the brace and the chord was determined. Due to the numerical analysis results the increase of thickness of the gusset plates did not result in the increase of the connection stiffness. However, the rotational stiffness of the tested connection influenced the truss stability.

The use of two-axis strength testing machines enabled the experimental tests. However, the load could only be applied in the limited range and the size of the samples had to be limited. The next research step is to carry out the process of optimization in terms of stiffness and load bearing capacity for that kind of connections. The appropriate connection stiffness between the purlin and the top chord determined during the design process may affect the reduction of additional braces located at the compressed bottom chord of trusses subjected to wind loading.

REFERENCES

[1] PN-EN 1993-1-1, Eurocode 3: Design of steel structures – Part 1-1: General rules and rules for buildings, 2005.

[2] A. Biegus, "Calculation of lateral bracing for cantilever and multispan girders", *Archives of Civil and Mechanical Engineering*, vol. 13, pp. 99-103, 2013, doi.org/10.1016/j.acme.2012.11.001.

[3] Sz. Pałkowski and M. Piątkowski, "About calculations of roof cross braces", *Engineering and Construction*, vol. 4, pp. 210-213, 2014.

[4] A. Biegus and D. Czepiżak, "Generalized model of imperfection forces for design of transverse roof bracings and purlins", *Archives of Civil and Mechanical Engineering*, vol. 18, pp. 267-279, 2018, doi.org/10.1016/j.acme.2017.07.002.

[5] D. Czepiżak and A. Biegus, "Refined calculation of lateral bracing system due to global geometrical imperfections", *Journal of Constructional Steel Research*, vol. 119, pp. 30-38, 2016, doi.org/10.1016/j.jcsr.2015.12.007.

[6] M. Krajewski, "Analysis of the influence of geometrical imperfections on the equivalent load stabilizing roof truss with lateral bracing system", *Journal of Theoretical and Applied Mechanics*, vol. 62, no. 2, pp. 231-240, 2024, doi.org/10.15632/jtam-pl/185163.

[7] E. Hotała and P. Hotała and M. Zambrowicz, "Safety of lattice purlins under wind or snow loads", in Proc. *LIII Scientific Conference by Committee of Civil and Water Engineering of the Polish Academy of Sciences*, vol. 2, Krynica, 2007, pp. 233-240.

[8] J. Jankowska-Sandberg, The influence of the lateral brace stiffness located at the compressed chord on the truss buckling loads", in Proc. *L Scientific Conference by Committee of Civil and Water Engineering of the Polish Academy of Sciences*, vol. 2, Krynica, 2004, pp. 221-228.

[9] J. Jankowska-Sandberg, *Selected stability problems of arch and truss girders*, ed. Koszalin University of Technology publishing house, Koszalin 2013.

[10] P. Iwicki, "Stability of trusses with linear elastic side-supports, *Thin Walled Structures*", vol. 45, pp. 849-854, 2007, doi.org/10.1016/j.tws.2007.08.005.

[11] P. Iwicki, "Sensitivity analysis of critical forces of trusses with side bracing", *Journal of Constructional Steel Research*, vol. 66, pp. 923-930, 2010, doi.org/10.1016/j.jcsr.2010.02.004.

[12] J. Jankowska-Sandberg and J. Kołodziej, "Experimental study of steel truss lateral torsional buckling", *Engineering Structures*, vol. 46, pp. 165-172, 2013, doi.org/10.1016/j.engstruct.2012.07.033.

[13] M. Piątkowski, "Experimental research on load of transversal roof bracing due to geometrical imperfections of truss", *Engineering Structures*, 242,11255, 2021, doi.org/10.1016/j.engstruct.2021.112558.

[14] M. Krajewski, "Stability of trusses with elastic side supports," PhD. thesis, Gdansk University of Technology, Poland, 2021.

[15] M. Krajewski and P. Iwicki, "Stability of an imperfect truss loaded by wind", *Engineering Transactions*, vol. 64, no. 4, pp. 509-516, 2016, et.ippt.gov.pl/index.php/et/article/view/729.

[16] M. Smak M and B. Straka, "Geometrical and structural imperfections of steel member systems", *Procedia Engineering*, vol. 40, pp. 434-439, 2012, doi.org/10.1016/j.proeng.2012.07.121.

[17] A. Biegus, "Trapezoidal sheet as a bracing preventing flat trusses from out-of-plane buckling", *Archives of Civil and Mechanical Engineering*, vol. 15, no. 3, pp. 735-741, 2015, doi.org/10.1016/j.acme.2014.08.007.

[18] M. Gajdzicki and J. Goczek, "Numerical simulation to determine torsional restraint of cold-formed Z purlin", *International Conference on Metal Structures*, Wrocław, 2011, pp. 424-433.

[19] *Femap with NX Nastran*, Instruction manual, Siemens Product Lifecycle Management Software INC., 2009

[20] R.H. Macneal, "A simple quadrilateral shell element", *Computers and Structures*, vol. 8, pp. 175-183, 1978.

[21] *Zwick/Roell BIAX Z20* strength testing machine, Instruction manual, www.zwickroell.com.

[22] *Sick* inclinometer, type TMM88A-PKC090, Instruction manual, www.sick.com/1073799

[23] *PMX* measurement amplifier, type 1-PX455, Instruction Manual, www.hbm.com/de/2981/pmx-modular-measuring-amplifier-system-for-the-iot.

[24] *QuantumX* measurement amplifier, type MX840B, Instruction manual, www.hbm.com/quantumx.

[25] G. Rakowski and Z. Kacprzyk, *Finite element Method in structural mechanics*, ed. Warsaw University of Technology publishing house, Warsaw 1993.